

**Experiments in Imaging Rupture Properties and Early Aftershocks of
Large Earthquakes**

FINAL TECHNICAL REPORT

Award 04HQGR0097

Peter M. Shearer
Institute of Geophysics and Planetary Physics
Scripps Institution of Oceanography
University of California, San Diego
La Jolla, CA 92093
858-534-2260 (phone), 858-534-5332 (fax)
pshearer@ucsd.edu

Program Element: III

*Research supported by the U.S. Geological Survey (USGS),
Department of the Interior, under USGS award number
04HQPA0001. The views and conclusions contained in this
document are those of the authors and should not be
interpreted as necessarily representing the official policies,
either expressed or implied, of the U.S. Government.*

Award 04HQGR0097

EXPERIMENTS IN IMAGING RUPTURE PROPERTIES AND
EARLY AFTERSHOCKS OF LARGE EARTHQUAKES

Peter M. Shearer Institute of Geophysics and Planetary Physics Scripps Institution of
Oceanography University of California, San Diego La Jolla, CA 92093 858-534-
2260 (phone), 858-534-5332 (fax) E-mail: pshearer@ucsd.edu

TECHNICAL ABSTRACT

In consultation with National Earthquake Information Center (NEIC) researchers, we investigate practical methods to routinely image rupture properties and very early aftershocks of large earthquakes. Our method will resolve the extent and duration of

faulting within 20 to 30 minutes following rupture initiation, using only stations that are available in real time. This will provide additional data about large earthquake sources beyond the routinely reported location, magnitude and moment tensor, improving the reliability of strong ground-motion predictions and tsunami warnings. Because our technique requires no prior assumptions about possible fault geometries and little to no human interaction, it is well suited for routine implementation. Results using global network data have proven successful for the 2004 M9.3 Sumatra-Andaman earthquake, the 2005 M8.7 Sumatra earthquake, the 2002 M7.9 Denali earthquake, and the 2001 M7.8 Tibet earthquake. In principle, the method should also return useful results for smaller earthquakes. Experiments to determine optimal station selection and filtering are continuing, but the current algorithm is already sufficiently proven that it is ready for immediate use. Release of a practical system will be facilitated by the fact that many of the codes are already tested and their further development will be performed in collaboration with NEIC researchers and tested on computers at the NEIC.

Award 04HQGR0097

EXPERIMENTS IN IMAGING RUPTURE PROPERTIES AND EARLY AFTERSHOCKS OF LARGE EARTHQUAKES

Peter M. Shearer Institute of Geophysics and Planetary Physics Scripps Institution of Oceanography University of California, San Diego La Jolla, CA 92093 858-534-2260 (phone), 858-534-5332 (fax) E-mail: pshearer@ucsd.edu

NON-TECHNICAL ABSTRACT

Currently the National Earthquake Information Center (NEIC) of the U.S. Geological routinely provides location and magnitude information for large earthquakes that are used by emergency response agencies to evaluate the probable areas of greatest damage. However, the location represents the point where rupture initiated rather than the point of greatest slip and thus may not be near the area of strongest ground shaking and maximum energy release. Recently, we have shown that back-projection of seismic waves can be used to directly image the rupture extent of large earthquakes. We are working to implement an operational version of our algorithms at the NEIC in order to provide fault rupture images to researchers within 20 to 30 minutes following earthquake initiation. This will make possible the release of more timely estimates regarding where the strongest shaking is likely to have occurred and the probability of tsunami generation. In the long run, our results will also provide basic knowledge about source processes and seismic wave propagation that will increase the ability of seismologists to make realistic forecasts regarding strong motion probabilities in different locations, thus contributing to the goal of reducing losses from earthquakes in the United States.

Results

Our back-projection method is a simplification of wavefield reverse-time migration, a tool for imaging structure in reflection seismology. For the j th source location, the seismograms are summed to make the stack s_j as a function of time t :

$$s_j(t) = \sum_k (p_k/A_k) u_k(t - t_{jk}^p + \Delta t_k),$$

where $u_k(t)$ is the vertical-component seismogram recorded at the k th station, and t_{jk}^p is the theoretical P -wave travel time from the j th source to the k th station (currently computed using the IASP91 velocity model). Δt_k denotes timing corrections obtained from waveform cross-correlation of the initial part of the P waves, which are used to enhance the coherence of the traces by accounting for effects due to 3-D structure. Finally, p_k and A_k are the polarity and amplitude of the seismograms obtained through cross-correlation analysis; the division by A_k insures that the traces have approximately equal weight. The stacking procedure sums the energy that is radiated from the given source point constructively and attenuates other energy present in the seismograms.

Filtering can be applied to the seismograms to enhance certain frequency bands but acceptable results are often obtained with simple demeaning of the traces. To ensure waveform similarity, only seismograms with a correlation coefficient for the initial P -wave of greater than a threshold value (typically 0.7) with respect to a waveform stack are included in the analysis. Starting windows for the cross-correlation are obtained using either predicted P arrival times or picks from an automatic picking algorithm (Earle and Shearer, 1994). The stacking is performed over an evenly spaced grid of source latitude and longitude, assuming a constant source depth. No prior assumptions are made regarding fault geometry. Differences in expected amplitudes from geometrical spreading, source depth variations and directivity effects are ignored, but they should be relatively minor.

The 26 December 2004 Sumatra-Andaman earthquake

The disastrous Sumatra-Andaman earthquake of December 26, 2004 was one of the largest ever recorded and generated a tsunami that killed hundreds of thousands of people. However, prediction of the tsunami was hampered by delays in recognizing the true magnitude and extent of the fault rupture. The initial NEIC body wave magnitude (determined automatically) was only 6.2. An hour later, this was increased to a surface wave magnitude of 8.5. The Harvard CMT solution of $M_w = 8.9$ (later adjusted to 9.0) was provided 6 hours after the earthquake. Clearly there is a need for a method that can quickly measure event size using the initial P -wave arrivals, rather than waiting for the slower surface wave arrivals.

The back-projection approach described above is such a method and can produce detailed images within 20 to 30 minutes of rupture initiation. It requires no prior knowledge of fault geometry, dimension, or rupture duration. In addition, this observation-driven method takes advantage of the entire P wavetrain and calculation of synthetic seismograms is not needed. It is insensitive to interference with later seismic phases such as PP , because their angle of incidence across the array is

different from direct P . Finally, our approach provides more detailed images of rupture timing and extent than simple measures of short-period P -wave duration versus azimuth such as those performed by Ni et al. (2005) for the Sumatran earthquake.

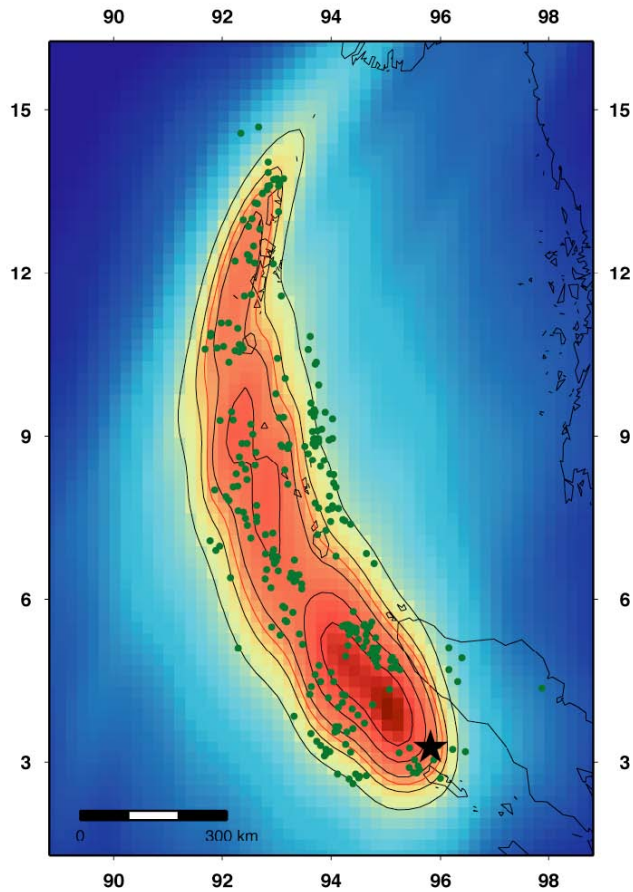


Figure 1. Seismic energy from the Sumatra-Andaman earthquake integrated over 600 seconds after initiation, normalised such that the maximum value is unity. The red contour, plotted at 65% of the maximum, encloses the slip area used to estimate the moment magnitude.

The epicenter is shown as the black star. Note the good agreement between the 1300-km-long rupture zone and the locations of the first month of aftershocks (dark green circles). The black contours are plotted at increments of 0.1 starting at 0.5. The image is computed and shown across the entire map but amplitudes are very weak outside the contoured region.

We first tested the method using data from the short-period Hi-Net seismic array in Japan. Our signal-to-noise cutoff resulted in 538 seismograms out of 686 available traces. Figure 1 shows the distribution of cumulative radiated energy in the 600 s from the start of the earthquake. The slip is greatest near the epicenter west of northern Sumatra, but there is also significant radiation in the northern portion west of Nicobar and Andaman Islands. The rupture is not confined to the southern part of the aftershock zone as some of the early finite slip models suggested. By studying the time dependence in these images, we find the rupture spread over the entire 1300-km-long aftershock zone by propagating northward at roughly 2.8 km/s for ~8 minutes.

Although the Japanese Hi-Net data provide the best images of this earthquake, useful results can also be obtained for Global Seismic Network (GSN) stations that are available in real time to the NEIC. Figure 2 shows results for the Sumatran earthquake, as obtained both using 112 global distributed stations and 47 stations located in Europe and the Middle East, at distances between 30 and 95 degrees from the hypocenter. We have generally found that superior results are obtained for very large earthquakes by using a regional subset of the global station distribution. Presumably this is a result of greater coherence with respect to 3-D velocity variations as the back-projected image moves away from the hypocenter. It may also involved complications arising from directivity and radiation pattern effects. Regardless, either approach would have quickly shown the roughly 1200-km long northward progression of the rupture from the epicenter within 30 minutes of the start of the Sumatra-Andaman earthquake.

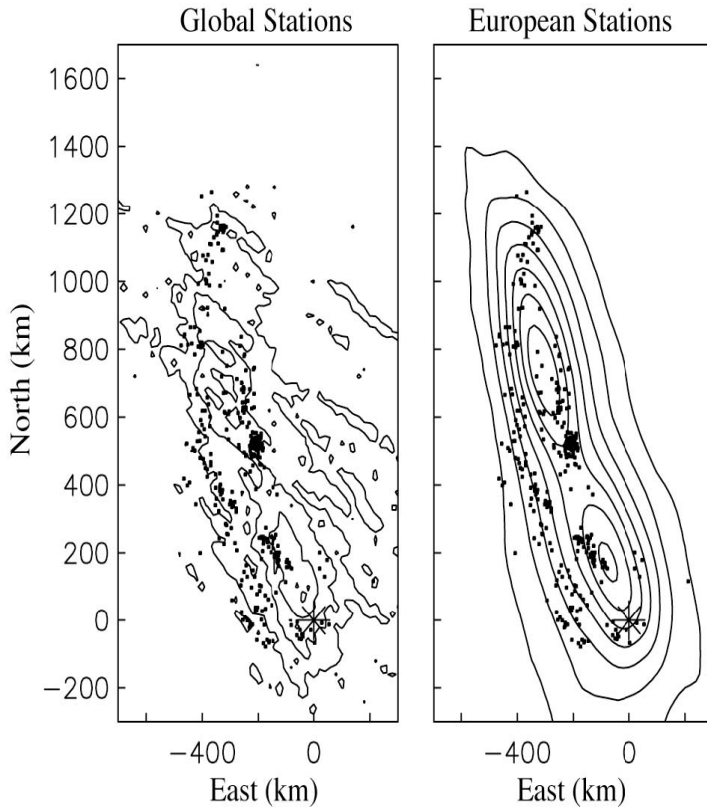


Figure 2. Images of the 2004 Sumatra-Andaman earthquake as obtained with a *P*-wave back-projection method for global seismic stations (left) and European stations only (right). The mainshock is the star at the plot origin; aftershock locations are shown as dots.

On March 28, 2005, another thrust event occurred with an estimated M_w of 8.7, about 300 km to the east-southeast of the December 26 earthquake. The surface shaking resulted in at least 2000 casualties, most of which were on the island of Nias about 100 km south-southeast of the hypocenter. This event did not produce a significant tsunami, as might have been expected based on the focal mechanism, which was nearly identical to that of the December M_w 9.3 event. However, this event was the second largest earthquake since the great 1964 Alaska earthquake.

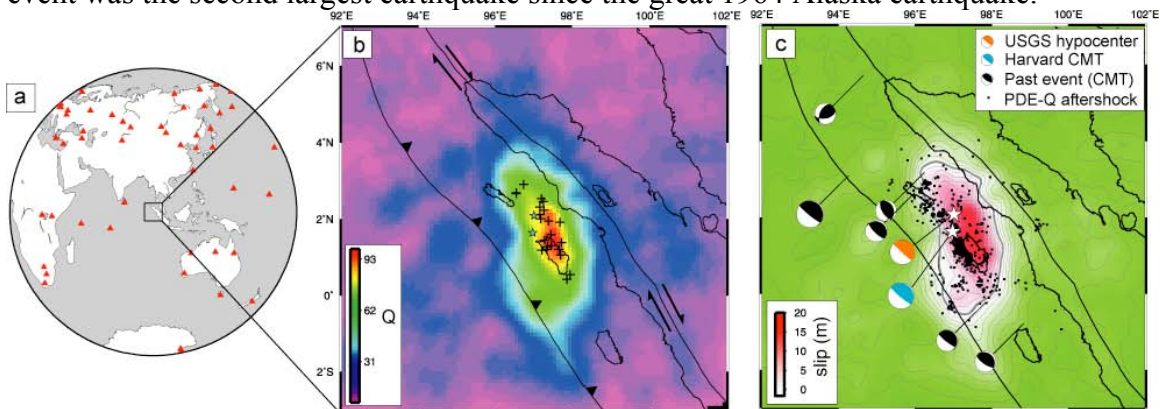


Figure 3. Images of back-projected *P*-wave energy for the March 28, 2005, $M_w = 8.7$ Sumatra earthquake. (a) The station distribution with respect to the epicenter. (b) Estimated relative seismic energy release with

plus symbols showing spatial centroids at different times. (c) Estimated slip using a simple energy/moment scaling relationship. Aftershock locations and selected focal mechanisms are also plotted. The thick gray contour outlines our estimate of the fault plane.

Results of the back-projection method applied to GSN stations are shown in Figure 3. Our resulting image agrees favorably with the distribution of the aftershocks and the location of the Harvard central moment tensor. The back-projected energy suggests that the rupture proceeded from the hypocenter in two directions: for a short distance toward the north and a much longer distance to the south. The observed *P*-wave radiation throughout the rupture zone is characterized by frequencies between 0.5 and 0.1 Hz. However, the seismic radiation in the south half of the rupture zone also contains lower frequencies (0.03 to 0.1 Hz), perhaps suggesting either temporal changes in rupture velocity or stress drop during rupture.

The 3 November 2002 Denali earthquake

The *M_w* 7.9 Denali earthquake in Alaska occurred within a region spanned by a well-instrumented local and regional seismic network. The rupture initiated on a north-dipping reverse fault and propagated eastward onto two additional strike-slip faults for a total distance of about 340 km and duration of about 120 s (Eberhart-Phillips et al., 2003; Ozacar et al., 2003). The average and maximum surface horizontal offsets are about 5 and 8.8 m, respectively (Haeussler et al., 2005). Based on seismic, GPS, and geological surface-offset data, the estimated total moment for the rupture ranges from 6.8 to 7.5×10^{20} Nm (Oglesby et al., 2005; Frankel, 2005; Hreinsdóttir et al., 2005). The first three hours of aftershocks detected by the networks ($M > 2.0$; Ratchkovski et al., 2003) span most of the rupture zone (Figure 4). This event was located in a sparsely populated area, leading to only minor injuries and structural damage.

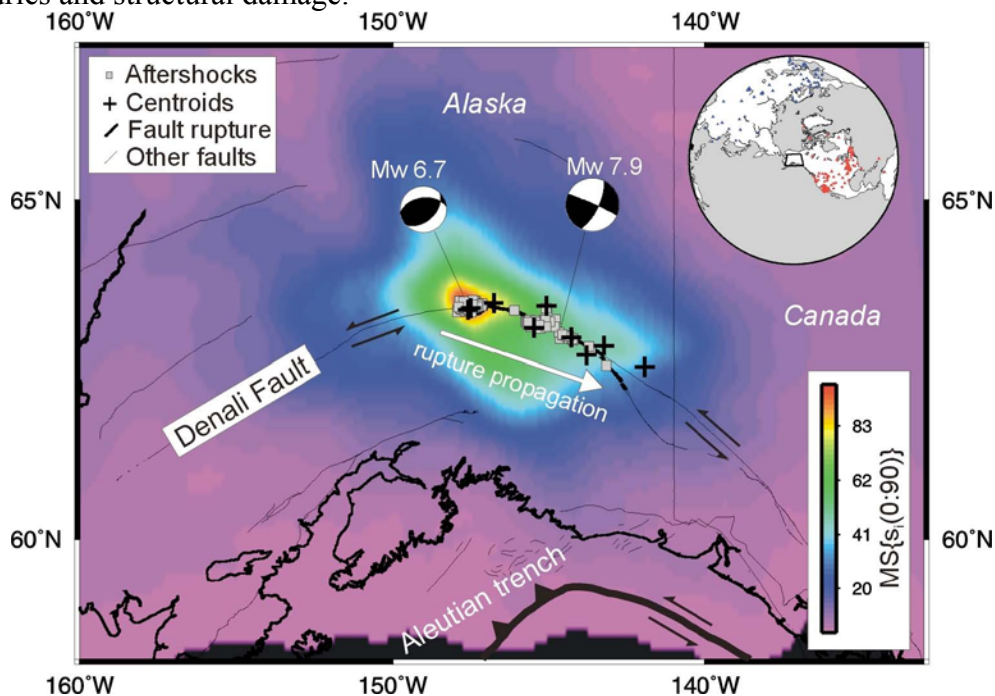


Figure 4. Image of the first 90 s of the Denali $M_w = 7.9$ earthquake as obtained with the back-projection method. Colors show contours of observed radiated seismic energy (MS). The PDE first-motion solution and Harvard CMT solution are shown. This image was created by stacking separate results from the North American stations (red) and the northern Eurasian stations (blue).

As in the case of the 2005 Sumatra earthquake (see above), we filter the data to between 2 and 30 s period. For the Denali earthquake, we find that improved waveform cross-correlation results can be obtained by applying a time-varying amplitude normalization algorithm to the P wave prior to computing the cross-correlations. The best source images are produced from using either continental US or European stations; the image plotted in Figure 4 is a stack of two separate source images obtained from these regions, integrated over the first 90 s of the event. In general, this image shows a peak near the hypocenter and a diffuse region extending to the east. Greater resolution can be obtained by plotting the image centroids in 10 s increments (as defined by the 80% of maximum contour in each time slice). These are plotted as the plus symbols in Figure 4 and closely track the Denali fault rupture.

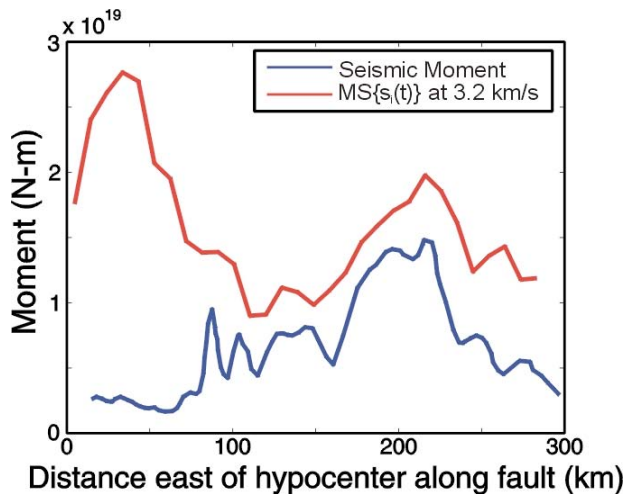


Figure 5. Back-projected energy $MS\{s(t)\}$ at centroids sampled every 3 s, compared with the along-strike moment model of Hreinsdóttir et al. (2005). The amplitude of MS is arbitrarily scaled for comparison purposes, but the spatial distribution is predicted by assuming the rupture initiates at the hypocenter and propagates unilaterally at 3.2 km/s.

The along-strike amplitude variation of the seismic moment model of Hreinsdóttir et al. (2005) correlates with our back-projection result, $MS\{s(t)\}$, sampled at centroids every 3 s (Figure 5). We assume that the rupture propagates unilaterally toward the east from the hypocenter at 3.2 km/s. Near the hypocenter the correlation breaks down, presumably because the technique forces greater coherence at the hypocenter. As one gets farther from the hypocenter, the coherence decreases due to a ray paths traversing different 3-D velocity structure to each station, causing $s(t)$ to decrease in amplitude. Complications in the imaging may also result from the fact that the Denali earthquake began as a thrust event (see PDE focal mechanism in Figure 4), which triggered strike-slip motion on the Denali fault where most of the moment was released. Thus the polarities obtained from cross-correlation of the initial P wave may not have been correct for later arrivals.

The 14 November 2001 Kokoxili earthquake

The $M_w = 7.8$ Kokoxili earthquake initiated on a 25-km long strike-slip fault and propagated 45 km northward across an extensional step-over onto the Kunlun strike-slip fault (Antolik et al., 2004). The rupture then propagated eastward for a total length of ~ 400 km, with an average and maximum surface horizontal offset of 2 m and 7.6 m (van der Voerd et al., 2002; Xu et al., 2002; Lin et al., 2003). The total duration and moment of the rupture was about 120 s and 5.3×10^{20} Nm (Antolik et al., 2004). The first three hours of detected aftershocks ($M > 3.5$) only occurred along two patches of the rupture zone, demonstrating the problem of using the aftershocks that immediately follow the mainshock to identify the rupture zone. However the remaining two months of aftershocks illuminate most of the rupture zone (Figure 6). This event was located in a very remote area, leading to little if any human injuries or structural damage.

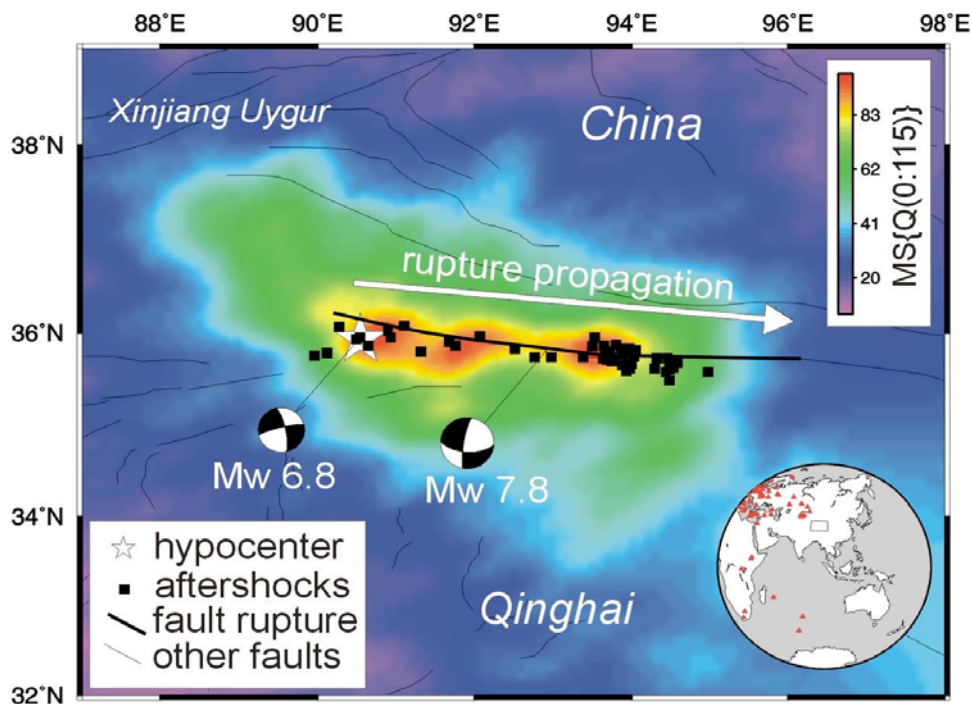


Figure 6. Image of the first 115 s of the Kokoxili $M_w = 7.8$ earthquake obtained from P -wave back-projection. Data are from GSN stations west of the study region (shown as the red triangles in the inset). The PDE first motion solution ($M_w = 6.8$) and Harvard CMT solution ($M_w = 7.8$) are plotted. The colors are contours of observed radiated seismic energy, with the region of highest energy (red) tracking the eastward fault rupture.

Our best back-projected image (Figure 6) is obtained using stations west of the earthquake, mostly consisting of European stations. The image shows the eastward rupture propagation along the Kunlun fault. In addition, the observed time dependence in our images roughly agrees with the rupture velocity and moment release obtained in other studies.

References

- Antolik, M., R. E. Abercrombie, and G. Ekström, The 14 November 2001 Kokoxili (Kunlunshan), Tibet, Earthquake: Rupture transfer through a large extensional step-over, *Bull. Seismol. Soc. Am.*, **94**, 1173-1194, 2004.
- Earle, P.S. and P.M. Shearer, Characterization of global seismograms using an automatic picking algorithm, *Bull. Seismol. Soc. Am.*, **84**, 366-376, 1994.
- Eberhart-Phillips, D., et al., The 2002 Denali Fault Earthquake, Alaska: A large magnitude, slip-partitioned event, *Science*, **300**, 1113-1118, 2003.
- Frankel, A., Rupture process of the M7.9 Denali Fault, Alaska, earthquake: Sub-events, directivity, and scaling of high-frequency ground motions, *Bull. Seismol. Soc. Am.*, in press, 2005.
- Haeussler, P. J., D. P. Schwartz, T. E. Dawson, H. D. Stenner, J. J. Lienkaemper, B. Sherrod, F. R. Cinti, P. Montone, P. Craw, A. J. Crone, and S. Personius, Surface rupture and slip distribution of the Denali and Totschunda faults in the November 3, 2002 M7.9 earthquake, Alaska, *Bull. Seismol. Soc. Am.*, in press, 2005.
- Hreinsdóttir, S., J. T. Freymueller, R. Bürgmann, and J. Mitchell, Coseismic deformation of the 2002 Denali Fault Earthquake: Insights from GPS measurements, *J. Geophys. Res.*, in press, 2005.
- Ishii, M., P.M. Shearer, H. Houston and J.E. Vidale, Rupture extent, duration, and speed of the 2004 Sumatra-Andaman earthquake imaged by the Hi-Net array, *Nature*, in press, 2005.
- Lin, A., M. Kikuchi, and B. Fu, Rupture segmentation and process of the 2001 Mw 7.8 central Kunlun, China, earthquake, *Bull. Seismol. Soc. Am.* **93**, 2477-2492, 2003.
- Ni, S., H. Kanamori and D. Helmberger, Energy radiation from the Sumatra earthquake, *Nature*, **434**, 582, 2005.
- Oglesby, D. D., D. S. Dreger, R. A. Harris, N. Ratchkovski, and Roger Hansen, Inverse kinematic and forward dynamic models of the 2002 Denali, Alaska earthquake, *Bull. Seismol. Soc. Am.*, in press, 2005.
- Ozacar, A. A., S. L. Beck, D. H. Christensen, Source process of the 3 November 2002 Denali fault earthquake (central Alaska) from teleseismic observations, *Geophys. Res. Lett.*, **30**, doi:10.1029/2003GL017272, 2003.
- Ratchkovski, N. A., R. A. Hansen, J. C. Stachnik, T. Cox, O. Fox, L. Rao, E. Clark, M. Lafevers, S. Estes, J. B. MacCormack, and T. Williams, Aftershock sequence of the Mw 7.9 Denali fault, Alaska, earthquake of 3 November, 2002 from the regional seismic network data, *Seismol. Res. Lett.*, **74**, 743-752, 2003.
- van der Woerd, J., A.-S. Mériaux, Y. Klinger, F. J. Ryerson, Y. Gaudemer, and P. Tapponnier, The 14 November 2001, Mw 7.8 Kokoxili earthquake in northern Tibet (Qinghai Province, China), *Seismol. Res. Lett.* **73**, 125-135, 2002.
- Walker, K., P. Shearer, M. Ishii and P. Earle, Telesismic imaging of the rupture zone of the 28 March 2005 Sumatra Mw 8.7 earthquake, *Geophys. Res. Lett.*, in preparation, 2005.
- Xu, X., W. Chen, W. Ma, G. Yu, and G. Chen, Surface rupture of the Kunlunshan earthquake (Ms 8.1), northern Tibetan plateau, China, *Seismol. Res. Lett.*, **73**, 884-892, 2002.